Solid State Sciences 12 (2010) 1953–1959

Contents lists available at ScienceDirect

Solid State Sciences

journal homepage: www.elsevier.com/locate/ssscie

In–$CuInS_2$ nanocomposite film prepared by pulsed laser deposition using a single source precursor

Wolfgang Bensch [a,*], Enrique Quiroga-González [a], Lorenz Kienle [b], Viola Duppel [c], Doh-Kwon Lee [d], Jürgen Janek [d]

[a] Institute for Inorganic Chemistry of the University of Kiel, Max-Eyth-Str. 2, 24118 Kiel, Germany
[b] Institute of Material Science of the University of Kiel, Kaiserstr. 2, 24143 Kiel, Germany
[c] Max Planck Institue for Solid State Research, Heisenbergstr. 1, 70569 Stuttgart, Germany
[d] Institute for Physical Chemistry of the University of Giessen, Heinrich-Buff-Ring 58, 35392 Giessen, Germany

ARTICLE INFO

Article history:
Received 28 April 2010
Received in revised form
19 July 2010
Accepted 8 August 2010
Available online 17 August 2010

Keywords:
In–$CuInS_2$
Nanocomposite film
Single source precursor
Pulsed laser deposition
Electrical properties
Photoconductivity

ABSTRACT

An In–$CuInS_2$ nanocomposite film has been prepared by Pulsed Laser Deposition applying a single source precursor. X-ray powder diffraction, Raman spectroscopy and transmission electron microscopy observations evidence that the film consists of nanocrystals of elemental In and chalcopyrite type $CuInS_2$ with sizes of 36 and 17 nm respectively. A detailed analysis of the electrical performance of the film suggests that the nanoparticles are in Ohmic contact and that the resistivity is mainly caused by the $CuInS_2$ nanocrystals which are less conducting than the pure In metal. Irradiation of the film with light shows a photoconductive effect mainly with wavelengths larger than 515 nm and smaller than 850 nm.

1. Introduction

$CuInS_2$ crystallizing in the chalcopyrite structure type is a material that has been extensively studied due to its good photoelectric properties [1,2]. It has a direct band gap of around 1.5 eV being in the optimum range for solar energy conversion [3], and can be prepared as both n- and p-type conducting material in bulk form [2,4], as films using various deposition techniques and starting materials [5–10], or as nanocrystals with quasi-spherical shape [11–13] or with different shapes like hollow microspheres [14], or nanotubes, nanoribbons and nanowires [15,16]. Recently, this material has been also used as core or shell of nanoparticles [17,18], and in the form of nanocolloids in nanocrystal inks for printable photovoltaics [19,20]. Despite many efforts the energy conversion efficiencies of solar cells prepared with this material have so far been limited to around 12% due to the difficulties to prepare films of very high quality [5,6]. Based on the pioneering work by Grätzel et al., Heeger et al. and others [21–25] new solar cell designs based on nanometre scale blends or so-called interpenetrating systems have been investigated. In many cases such nanosized or nanostructured cells work with dye-electrolyte couples or organic materials. The disadvantages of these cells are the risk of leakage and degradation. Therefore, there is a need of pure inorganic materials for such nanostructured solar cells and one approach is the usage of inorganic nanoclusters together with $CuInS_2$. For example, nanocomposite films of TiO_2 and $CuInS_2$ have been prepared by chemical spray deposition to produce a nanocomposite 3D solar cell. The TiO_2 nanoparticles reduce the migration distance of the minority carriers during photoconduction and in that way also the recombination rate resulting in an improvement of the efficiency [26,27]. The performance of such nanocomposite solar cells is strongly influenced by several parameters like buffer layer thickness or morphology of the TiO_2 nanoparticles [27]. Despite some promising results on this kind of nanocomposites, they have not been much explored, even when there are other good candidates to form nanoclusters in $CuInS_2$.

Very recently it was demonstrated that In metal deposited on $CuInS_2$ films shows the lowest specific contact resistivity which is of great importance for solar device properties [28]. Such a low contact resistance of In with $CuInS_2$ could be beneficial in

* Corresponding author. Tel.: +49 431 8802094.
E-mail address: wbensch@ac.uni-kiel.de (W. Bensch).

1293-2558/$ – see front matter © 2010 Elsevier Masson SAS. All rights reserved.
doi:10.1016/j.solidstatesciences.2010.08.005

composite systems for photoconductive applications. On the other hand, tandems of nanometric layers of metals with semiconductors exhibit interesting photoconductive properties with ballistic transport of photo-excited carriers through the metal layers [23,29]. These observations encouraged us to synthesize nanocomposite films containing $CuInS_2$ and In nanoparticles. The concept of metal-semiconductor nanocomposite films is new and we started to develop a suitable synthesis strategy. For the synthesis a single source inorganic-organic precursor was used, because in this state the elements are mixed on atomic level. The precursor material $[C_{13}H_{28}N_2]_5Cu_{2.1(1)}In_{17.9(1)}S_{33}\cdot 17H_2O$ was selected because it contains only Cu, In and S besides the organic molecules and water. Furthermore, the In:Cu ratio is high increasing the possibility of deposition of elemental In besides a Cu–In–S phase thus forming the desired nanocomposite. In addition, the present investigation should show whether such a compound composed of large inorganic clusters is suitable as a single source precursor. The selected deposition method was PLD where the fast ablation of the target material by the excimer laser minimizes the preferential vaporization of the different elements, allowing the production of homogeneous films in a broad range of thicknesses [30].

During the deposition process of the film regularly distributed $CuInS_2$ and In nanoparticles were formed. The nanocomposite film was characterized with respect to the structural, optical and photoelectric properties and the results are presented and discussed in the paper. The film was analyzed by Raman spectroscopy, X-ray powder diffraction (XRD), high resolution transmission electron microscopy (HRTEM), UV–vis spectroscopy and by means of *I–V* (current–voltage) measurements.

2. Experimental details

2.1. Preparation of the precursor

An hybrid (organic-inorganic) Cu–In open framework thiometalate with composition $[C_{13}H_{28}N_2]_5Cu_{2.1(1)}In_{17.9(1)}S_{33}\cdot 17H_2O$ (**1**), isostructural to the known framework with composition $[C_{13}H_{28}N_2]_5Cd_4In_{16}S_{33}\cdot 13H_2O$ [31] was prepared. Note that the estimated variation of the composition of the compound is based on the average of several analyses performed on different batches. For the synthesis, 0.7 mmol of CuS, 4.2 mmol of In, 6.9 mmol of S and 13.46 mmol of 4, 4′-trimethylenedipiperidine were used. The precursors were mixed with 2.5 mL of water and 2.5 mL of ethyleneglycol in a 35 mL Teflon-lined stainless steel autoclave and stirred for 15 min. The sealed vessel was then heated at 190 °C for 5 days. After cooling down to room temperature, the product was filtered off, and washed with water, ethanol and acetone. Prismatic yellow crystals in a yield larger than 90% based on In were obtained. Details of the structure and properties of the compound $[C_{13}H_{28}N_2]_5Cu_{2.1(1)}In_{17.9(1)}S_{33}\cdot 17H_2O$ will be published elsewhere.

The product was crushed and the obtained powder was thermally treated in Argon atmosphere at 330 °C for 2.5 h. After decomposition of the precursor material elemental analysis gave 15 weight% of C. The black amorphous product was finally pressed isostatically to form a pellet being 1.5 cm long and 1 cm in diameter. This pellet was used as the single source precursor for the deposition of the film.

2.2. Deposition of the film

The film was deposited by pulsed laser deposition (PLD) on a (111) Si substrate with resistivity $100 \cdot 10^3$ Ωcm heated at 500 °C, under vacuum. We used a vacuum chamber (minimum pressure $p = 5\cdot 10^{-3}$ Pa) equipped with a turbomolecular pump and a cold trap (liquid nitrogen) to avoid a sulfur contamination of the pumping system. A Kr-F excimer laser ($\lambda = 248$ nm, Compex 201, Lambda-Physik, Göttingen, Germany) was used for the ablation process. For the deposition, the optimized conditions for the preparation of good quality films of other chalcogenide composites were used [30,32]. We chose pulse energy of 160 mJ, corresponding to approximately 4 J/cm^2. The repetition rate was adjusted to 5 Hz, the pressure of the background gas was fixed to 1 Pa, and the substrate temperature was 500 °C. Argon was used as the background gas. The distance between the target and the substrate was adjusted to 40 mm. The thickness of the films was estimated as approx. 3 μm.

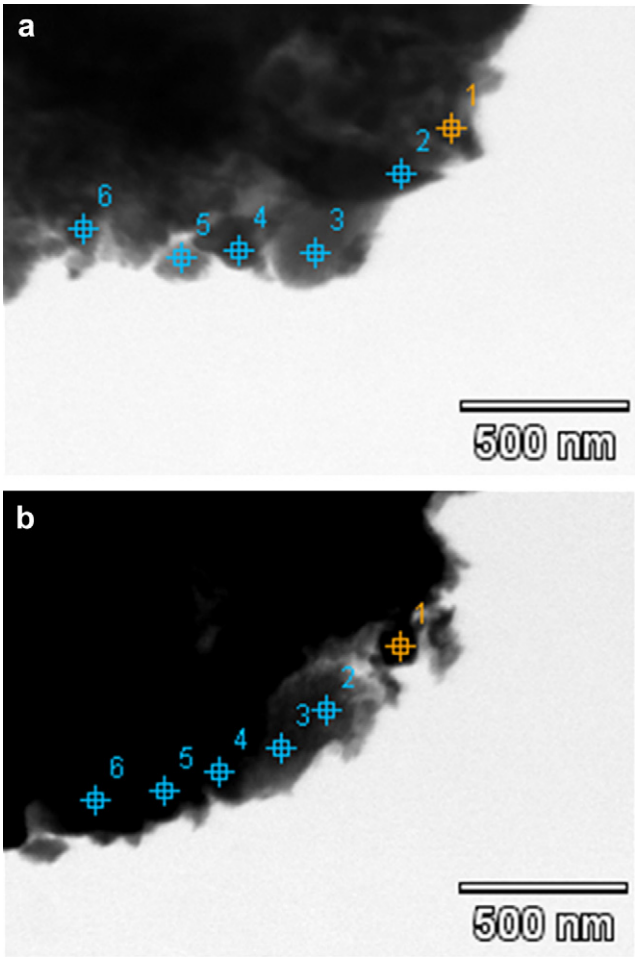

Fig. 1. TEM micrographs of a) an In-rich zone and b) a S-rich zone. EDX analyses were done in the indicated points and the results are summarized in Table 1.

2.3. Characterization methods

For Transmission Electron Microscopy (TEM) investigations, the film was scratched from the substrate and the resulting micro-particulates were transferred to aluminium grids which were fixed in a side-entry, double-tilt holder with the tilting limited to a maximum of ±25° in two directions. High resolution transmission electron microscopy (HRTEM) was performed with a Philips CM30ST (300 kV, LaB_6 cathode). EDX (energy dispersive X-ray spectroscopy) was performed in the scanning and nanoprobe mode of the CM30ST instrument using a Si/Li-EDX detector (Noran, Vantage System).

Table 1
EDX analyses in at.% of a) an In-rich zone and b) a S-rich zone, which are illustrated in Fig. 1 a) and b)

Zone	Point	S–K	Cu–K	In–L
a)	1	25.8	9.4	64.8
	2	6.0	2.0	92.0
	3	35.3	13.8	51.0
	4	10.3	4.0	85.7
	5	34.2	9.9	56.0
	6	9.3	2.8	87.9
b)	1	29.3	4.6	66.2
	2	47.7	8.0	44.3
	3	51.8	8.2	40.0
	4	51.4	8.4	40.2
	5	40.1	5.8	54.0
	6	50.5	7.4	42.0

XRD (X-ray Diffractometry) measurements were performed with a PANalytical X'PERT-PRO diffractometer in reflection mode using Cu–Kα radiation. The diffractogram was collected in the 2θ range from 31 to 58° to avoid the reflections from the Si substrate. The Raman spectrum of the film was measured with a HORIBA Jobin Yvon Xplora microscope, using 638 nm laser excitation, a 100x Olympus objective with 0.9 numerical aperture, and an 1800 groove/mm grating with a spectral resolution of about 1.2 cm^{-1}. Approximately 10 mW laser light was focused on the sample in order to avoid artefacts in the measurements due to heating. Measurements of optical reflection were carried with a Cary 5000 UV–Vis–NIR spectrophotometer in the range of 200–900 nm, using a halogen lamp as light source and a photomultiplier as detector. The *I–V* characteristics of the film were measured with a source–measure–unit Keithley 236 in sweep mode under darkness and under illumination. A 250 Watt Long Life Metal-Halogenide lamp was used as light source, providing a light power of 4 mW/cm^2 to the surface of the sample. A two probe arrangement was used for the measurements with every probe serving as a current and as a voltage probe, contacting directly the surface of the film. The diameter of the probes was around 0.2 mm. The distance between probes for the measurement was either 0.5 or 2.5 mm.

3. Results and discussion

3.1. Structural and chemical characterization

Microprobe EDX analyses performed in the scanning electron microscope show the atomic ratio of Cu : In : S is as expected from the precursor. However, according to nanoprobe EDX measurements performed in TEM, the ratio of the constituting elements Cu, In, S varies strongly and unsystematically at the nanoscale. Hence, nanoprobe analyses were undertaken to figure out the reason for the large compositional fluctuations. In the TEM images displayed in Fig. 1a and b the different numbered spots indicate the areas where EDX analyses were carried out. The micrograph in Fig. 1a was recorded in an In-rich area whereas the picture shown in Fig. 1b was taken in a S-rich region. The results of the analyses summarized in Table 1 clearly evidence that in the In-richest regions only small amounts of S and Cu are present. The large compositional variation is caused by the nanodisperse distribution of the components well seen in the TEM micrographs, e.g. $CuInS_2$, In and amorphous S. The latter together with remaining carbon might represent the amorphous areas between the nanocrystals. No evidence for secondary crystalline phases in the film were obtained as described below.

A part of the Raman spectrum of the film is shown in Fig. 2. The Raman peak centered at 310 cm^{-1} is blue-shifted with respect to

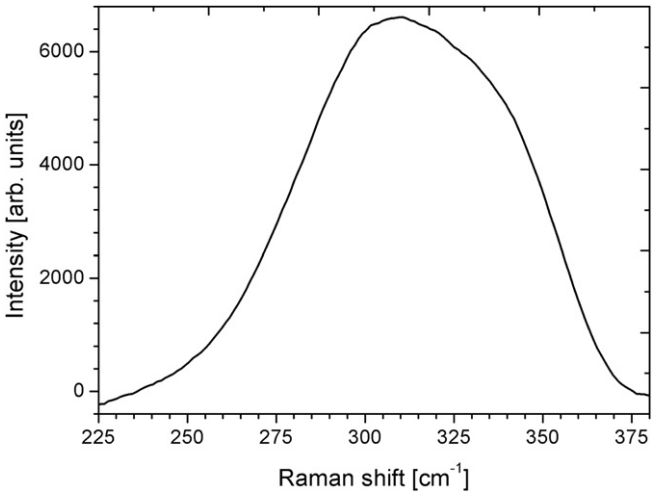

Fig. 2. Raman spectrum of the film. The peak centered at 310 cm^{-1} is due to the A_1 phonon mode of $CuInS_2$. The broadness of the peak indicates the nanocrystalline nature of the film.

the position of the A_1 phonon mode of bulk $CuInS_2$ positioned at around 290 cm^{-1} [33]. This effect has been reported for In-rich $CuInS_2$ films [34]. In the present film the shift of the mode is due to the nanosized In particles found together with $CuInS_2$. The width of the peak is an indication of the nanocrystalline nature of the material, and the asymmetry is caused by the size distribution of the nanocrystals, as in the case of nanocrystalline Si [35]. The presence of $CuIn_5S_8$ which is a common byproduct in $CuInS_2$ films [36] could be discarded since its Raman line is located at 362 cm^{-1} [37], exactly at the edge of the Raman peak centered at 310 cm^{-1}. On the other hand, $CuInS_2$ with CuAu structure type presents a Raman peak at 305 cm^{-1} [6] which is very close to the experimentally determined position of 310 cm^{-1}. Nevertheless this structure type of $CuInS_2$ is not in accordance with the XRD and electron diffraction (ED) patterns.

The TEM bright-field image (Fig. 3a) shows an area containing $CuInS_2$ nanocrystals (nCs). The crystalline particles are enclosed in white lines in the figure, an as can be seen they are randomly oriented. Fourier transforms of different TEM micrographs were performed yielding patterns with the *d*-values of $CuInS_2$ with chalcopyrite structure. The nCs are uniformly distributed and are separated by amorphous regions (thinner than 1 nm), which contain carbon and possibly sulfur. The sizes of the nCs range between 13 and 20 nm. In Table 2 are listed the *d*-values calculated from the ED pattern of Fig. 3b and those of bulk chalcopyrite $CuInS_2$ [38] and $CuInS_2$ with CuAu structure [39]. A comparison of the data clearly demonstrates that the $CuInS_2$ crystallites in the film have very similar lattice parameters like bulk $CuInS_2$ with the chalcopyrite structure type [38]. A further comparison with the *d*-values expected for the CuAu structure type of $CuInS_2$ [39] evidences the absence of this structure type in the film material, especially because the observed *d*-value close to 0.32 nm is not present in the CuAu structure type. Therefore, the analysis of the ED pattern supports that the nCs are $CuInS_2$ with chalcopyrite structure and that the Raman peak at 310 cm^{-1} corresponds to the A_1 phonon mode of this material. This conclusion is further evidenced by the detailed analysis of the XRD pattern.

The XRD pattern of the film is displayed in Fig. 4. The most intense reflections located at $2\theta = 32.9, 36.3, 39.2, 54.5$ and 56.6°, correspond to the (101), (002), (110), (112) and (220) planes of elemental In [40]. The reflections are significantly broadened, which could be caused by strain and/or particle size effects. The particle size of the coherent scattering domains of the In clusters

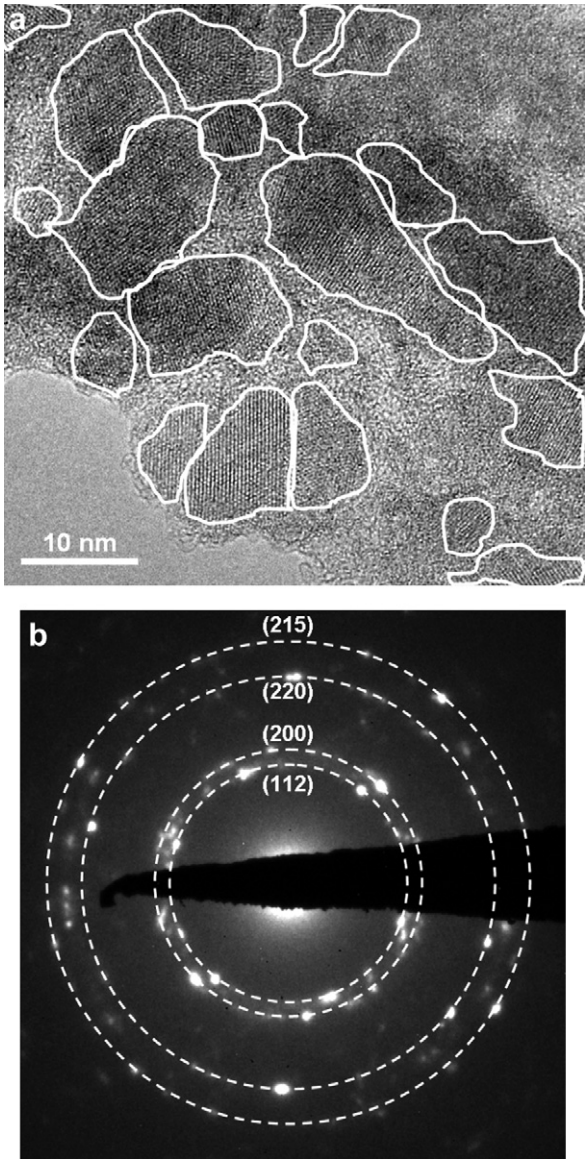

Fig. 3. a) TEM micrograph of a region of the film containing $CuInS_2$. This material consists of randomly oriented nanocrystals (enclosed in white lines). b) Electron diffraction pattern measured in this region.

calculated with the Debye–Scherrer formula is about 36 nm using the (101) reflection (no correction was made for instrumental broadening). The two Bragg peaks located at 46.8 and 55.4° can be indexed with the (220) and (215) reflections of chalcopyrite $CuInS_2$ which were reported to occur at 46.84 and 55.36° 2θ [38]. Several intense reflections of $CuIn_5S_8$ like the (511/333) at 43.99 and the (440) at 48.13° 2θ are not seen in the pattern [41], highly suggesting the absence of this material in the film. Again, the full-width at half

Table 2
d-values extracted from the electron diffraction pattern together with those of chalcopyrite and CuAu type $CuInS_2$.

d [nm] meas.	Planes $CuInS_2$ chalc.	*d* [nm] $CuInS_2$ chalc.	Planes $CuInS_2$ CuAu type	*d* [nm] $CuInS_2$ CuAu type
0.317	(112)	0.3157		
0.305	(103)	0.3037	(002)	0.3078
0.192	(220)	0.1938	(003)	0.2053
0.164	(215)	0.1658	(004)	0.1538

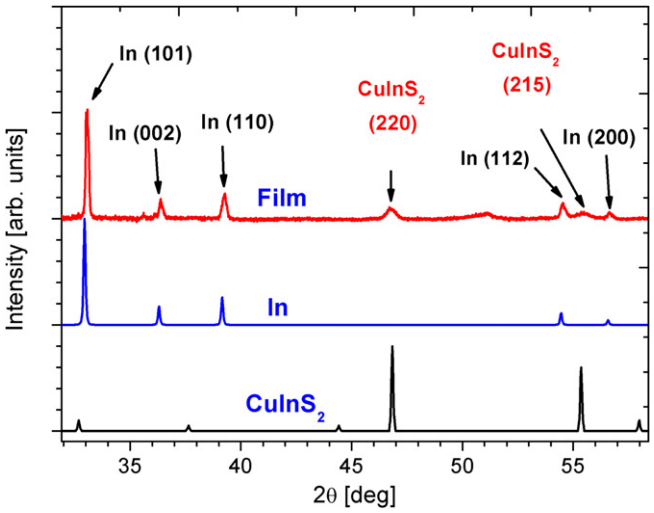

Fig. 4. X-ray powder pattern of the $CuInS_2$/In film. The most intense reflections originate from In nanoclusters. The broad Bragg peaks at 46.8 and 56.4° are due to nanocrystals of chalcopyrite $CuInS_2$.

maximum was used to calculate the crystallite size of the $CuInS_2$ nanoparticles and a value of 17 nm is obtained. The crystallite sizes determined from the powder pattern are in good agreement with the sizes estimated from the TEM picture. The very broad feature in the pattern located around 51.2° 2θ cannot be explained by any Cu–In–S, In–S and/or Cu–S phase, and its origin is still not clear. Considering the areas of the most intense reflection peaks of In and $CuInS_2$ an approximated ratio of 7:1 of In:$CuInS_2$ is calculated, in good agreement with the expected ratio of 8:1.

3.2. Optical and photoelectrical characterization

From the optical reflectance measurements and considering zero transmission, the percentage of absorption can be calculated with the simple relation

$$A = 100(1 - R) \quad (1)$$

with A being the percentage of absorption and R the reflectance. The optical absorption spectrum of the sample is shown in Fig. 5 and the inset of the figure displays the absorption spectrum from the Si substrate for comparison. In the considered energy range the absorption of the Si substrate decays monotonically with increasing energy, contrary to what is found for the sample. Despite the contribution of the substrate to the absorption spectrum, an absorption edge is evident in the plot caused by the material of the film. The absorption edge at around 1.46 eV is close to the optical band gap E_g of bulk $CuInS_2$ of 1.5 eV [2]. We note that the value for E_g reported in literature scatters between 1.4 and 1.77 eV depending on the synthesis conditions, Cu:In ratio, particle size, or post-synthesis treatments. $CuInS_2$ nanocrystals prepared by a solution-based method exhibit E_g values either smaller than 1.5 eV (1.47 eV) [42] or much larger (1.65–1.77 eV) [43]. It has been also reported that the value of E_g of $CuInS_2$ films could vary from 1.4 to 1.47 eV increasing the annealing temperature [44]. Such a large variation has been also observed for films changing the Cu:In ratio between 1.2 and 0.9 [45]. Some examples for the variation E_g depending on the synthesis method are 1.51 eV for films prepared by sulfuration of Cu/In stacks [46], 1.53 eV for crystalline powders prepared by a sintering method [47] and 1.4 eV for sprayed films [48]. The E_g value for $CuIn_5S_8$ is lower than the values for $CuInS_2$, and is commonly around 1.3 eV [49,50].

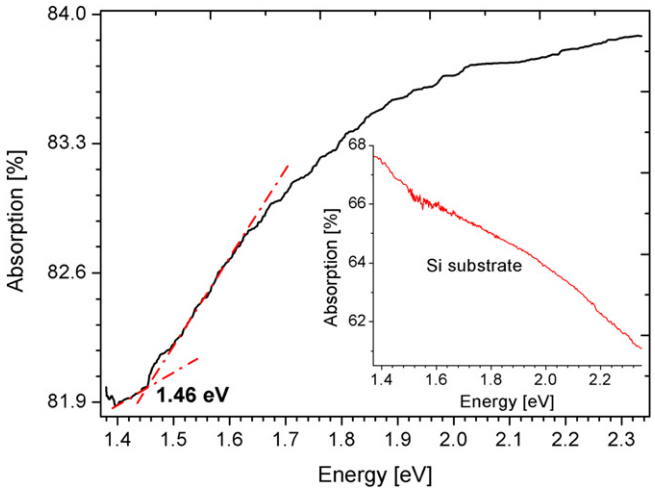

Fig. 5. Absorption spectrum of the film. The absorption edge is at around 1.46 eV. The absorption spectrum from the Si substrate is shown in the inset of the figure, for comparison.

The current–voltage (I–V) characteristics of the film under darkness and illumination are displayed in Fig. 6. The shape of both curves is typical for ohmic behavior, i.e. the contacts and the In nanoclusters in the film present a negligible electrical resistance [51], allowing the control of the current by the resistivity of $CuInS_2$. The photosensitivity $\Delta I/I_0$ with ΔI being the photocurrent and I_0 the dark current, both determined applying the same voltage, calculated from the curves yields 0.455. Examples of reported values of the photosensitivity of Cu-poor $CuInS_2$ are 0.1 for single crystals [2] and 1 for sprayed pyrolized films [52]. This parameter is not affected when a filter of 515 nm is used in front of the lamp. This result suggests that the film exhibits photoconductive effects mainly under light with wavelengths larger than 515 nm and smaller than 850 nm (1.46 eV, the band gap of the material). This photoresponse band is close to that of $CuInS_2$ films reported in other works [1].

The resistance of the film, calculated from the I–V plot under darkness is 219.4 kΩ. This resistance (R_t) of the sample combines the contributions of the probe resistance (R_p), the contact resistance (R_c), spread resistance (R_{sp}) and the resistance of the film (R_s), as described in equation (2).

$$R_t = 2R_p + 2R_c + 2R_{sp} + R_s \quad (2)$$

The values for R_p, R_c and R_{sp} are independent of the distance between the contacts, while R_s varies linearly with the contact distance. This dependency was checked by measuring the resistance with a distance between contacts 5 times larger (2.5 mm) yielding a value for R_t of 371.4 kΩ (R_{t1}). With this distance the value for R_s is supposed to be 5 times larger, and equation (1) can be rewritten as:

$$R_{t1} = 2R_p + 2R_c + 2R_{sp} + 5R_s \quad (3)$$

Solving the system of equations (1) and (2) gives $R_s = 38$ kΩ. The rest of the resistance is due to the other contributions, but as the resistance R_p is around 5 Ω and $R_c << R_{sp}$ because the contact is ohmic, R_{sp} could be considered to be the major contribution for the resistance, and for the value $R_{sp} \approx 181.4$ kΩ is derived. From this value it is possible to estimate the resistivity. For semi-infinite thick films, the resistivity can be calculated with the relation [53]:

$$R_{sp} = \rho/4r \quad (4)$$

where r is the radius of the probe. The estimated electrical resistivity using relation (4) amounts to $7.2 \cdot 10^3$ Ωcm, which is in the range of values reported for stoichiometric and In-rich $CuInS_2$ films (n-type films) [54,55]. We want to mention that according to some reports the value of the resistivity may be overestimated by a factor that depends on the ratio r/th, with th being the thickness of the film [56]. In the present case an overestimation of the resistivity by up to two orders of magnitude cannot be excluded, and therefore the calculated value of the resistivity should be regarded as an approximation. It is also worthy to mention that a survey of resistivity data published in literature for $CuInS_2$ demonstrates that the data scatter over a relatively wide range. Important factors controlling the resistivity are the synthesis method, chemical composition and type of material, i.e., whether experiments were conducted on bulk or films. For instance, an n-type $CuInS_2$ film deposited on glass using thermal evaporation of suitable ingots in a high-vacuum chamber exhibits a resistivity of $5.5 \cdot 10^2$ Ωcm [7] which varies up to three orders of magnitude varying the annealing temperature from 300 to 500 °C [57]. A strong dependence of the electrical resistivity on the Cu:In ratio was observed for films deposited by spray pyrolysis [39] and other methods. By this technique In-rich $CuInS_2$ films composed of very small crystallites contain In_6S_7, In_2S_3 and $CuIn_5S_8$ as impurity phases. Such films show electrical resistivity values around 10^6 Ωcm. A significant drop of the resistivity to about 0.06 Ωcm occurs for Cu:In ratios around 0.9–1.2 where the impurity phases could not be detected in X-ray powder patterns, and additionally the material becomes p-type conducting (In poor) [39]. Using chemical bath deposition for the preparation of p-type $CuInS_2$ films yields 51 Ωcm after annealing of the film at 450 °C in a sulfur atmosphere [6]. For sputter deposited p-type films the electrical resistivity has been reported ranging from 10^{-1} to 10^1 Ωcm depending on the post-treatment of the as-deposited films [38]. Other groups have reported a change of n-type to p-type in sputtered films upon aging in air, having then a change in resistivity of $2 \cdot 10^4$ to 10^{-1} Ωcm [58]. For stoichiometric polycrystalline $CuInS_2$ bulk material prepared under high-pressure high-temperature conditions the electrical resistivity is roughly 30 Ωcm [5]. On the other hand, highly densified and oriented stoichiometric $CuInS_2$ single-crystal fragments synthesized by sintering at 1050 °C have a resistivity of 50 Ωcm [4].

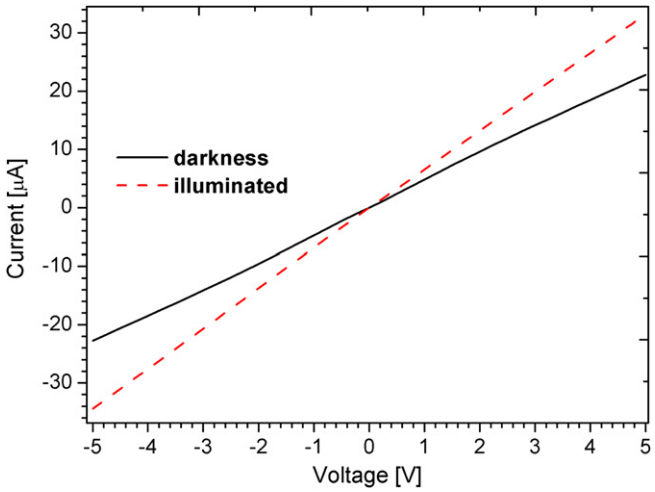

Fig. 6. I–V curves from the film under darkness and under illumination. The distance between contacts was 0.5 mm.

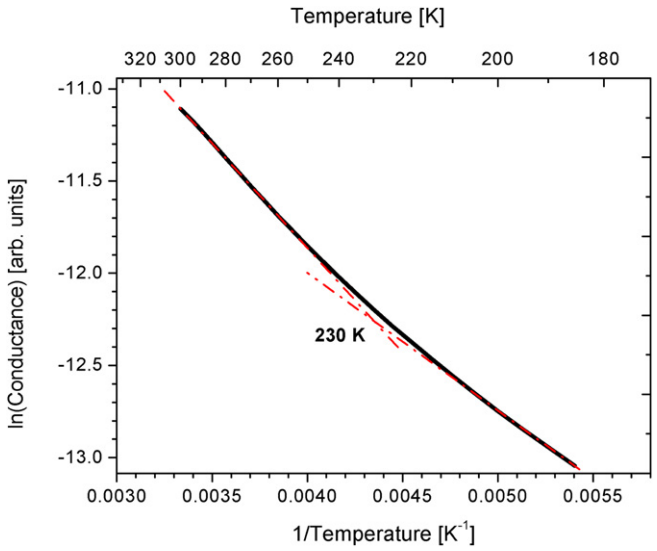

Fig. 7. Plot of ln(conductance) of the film versus 1/Temperature. There is a transition of the slope around 230 K. Above this temperature the conductivity is dominated by band-to-band transitions. Below 230 K the impurities of the material start to be more important for the electrical conduction.

In the present film a larger value for the resistivity could be expected considering the large amount of defects due to the grain boundaries of the $CuInS_2$ nCs [54], and due to the presence of amorphous C at the interfaces. But it seems that In nanoclusters and the $CuInS_2$ particles have a reasonable good contact so that scattering phenomena of the carriers at the large number of interfaces are relatively low. Because the resistivity of In metal is much smaller than the resistivity of $CuInS_2$, the main contribution to the resistivity should be due to the $CuInS_2$ nanocrystals.

A temperature-dependent I–V study of the film was done to confirm the semiconducting behavior. For semiconductor materials it is well known that the conductivity σ varies exponentially with the temperature according to:

$$\sigma = \sigma_0 \exp \frac{-E_g}{2kT} \quad (5)$$

where σ_0 is an overall constant that depends on the mobility, E_g is the band gap, k is the Boltzmann constant and T is the Temperature in K. When plotting $\ln(\sigma)$ versus 1/T the obtained curve is linear. Changes of the slope occur if impurities are present in the material. These impurities need less energy to be activated.

In Fig. 7 a plot of ln(conductance) of the film versus temperature is presented. As can be seen, the curve is linear from 300 to 230 K. In this region the conductivity is dominated by band-to-band transitions. Below 230 K the slope changes and below this temperature the impurities start to be more important for the electrical conduction. The transition at 230 K is in good agreement with the value of 250 K reported for n-type $CuInS_2$ [2]. Such a transition was also observed in the material with p-type conductivity [59,60].

4. Conclusions

A metal-semiconductor nanocomposite film consisting of nanocrystals of $CuInS_2$ with chalcopyrite structure and of In nanoclusters was prepared by PLD using a single source precursor. The new synthesis approach bases on a two-step procedure. The Cu-poor $[C_{13}H_{28}N_2]_5Cu_{2.1(1)}In_{17.9(1)}S_{33}\cdot 17H_2O$ thiometalate was prepared solvothermally in the first step followed by controlled thermal decomposition. According to the TEM and X-ray diffraction experiments the size of the $CuInS_2$ crystallites in the film is around 17 nm. The X-ray powder pattern indicates that the In particles are slightly larger than those of $CuInS_2$. An interesting aspect of the synthetic approach is the occurrence of $CuInS_2$ and elemental In despite the large deviation of the Cu:In ratio from 1:1 in the precursor material. In several contributions it was demonstrated that small deviations from the stoichiometric 1:1 ratio for Cu:In lead to the formation of different sulfides as impurity phases thus significantly changing the electrical characteristics of the films. At the moment we have no simple explanation for our experimental finding.

Despite the nanoscale crystals and the large number of defects and grain boundaries the electrical and photoelectrical properties of the film are comparable with $CuInS_2$ films prepared with different synthesis methods and without In nanocrystals. Especially the electrical resistivity is in the same order of magnitude as reported in literature for high quality $CuInS_2$ films. This result is somewhat surprising and one possible reason for the relatively good conductivity is the presence of In nanoparticles being in good contact with the $CuInS_2$ crystallites, i.e., the scattering at the particle interfaces is low. Additionally, as the resistivity of In metal is much smaller than the one of $CuInS_2$, the main contribution to the resistivity should be due to the $CuInS_2$ nanocrystals. One would also expect some short circuits between In nanoparticles. But due to the particle distribution such short circuits are statistical and there is not a direct In metal pathway for the electrical current in the film, as confirmed by the electrical measurements.

Further experiments are under way for the synthesis and characterization of thin films using different precursors and applying the PLD technique.

Acknowledgements

The authors appreciate the support of CONACyT and DAAD. The TEM experiments were enabled by Prof. Dr. Dr. h.c. mult. A. Simon at the Max Planck Institute for Solid State Research.

References

[1] L.L. Kazmerski, C.C. Shieh, Thin Solid Films 41 (1977) 35.
[2] D. Cybulski, A. Opanowicz, Cryst. Res. Technol. 32 (6) (1997) 813.
[3] E. Bucher, Appl. Phys. 17 (1978) 1.
[4] N. Yamamoto, J. Ogihara, H. Horinaka, Jpn. J. Appl. Phys. 29 (1990) 650.
[5] K. Yoshino, K. Nomoto, A. Kinoshita, T. Ikari, Y. Akaki, T. Yoshitake, J. Mater. Sci. Mater. Electron. 19 (2008) 301.
[6] F. Cui, L. Wang, Z. Xi, Y. Sun, D. Yang, J. Mater. Sci. Mater. Electron. 20 (2009) 609.
[7] M. Ben Rabeh, N. Chaglabou, M. Kanzari, Chalcogenide Lett. 6 (2009) 83.
[8] C. Calderon, P. Bartolo-Perez, J. Clavijo, J.S. Oyola, G. Gordillo, Sol. Energy Mater. Sol. Cells 94 (2010) 17.
[9] S. Seeger, K. Ellmer, Thin Solid Films 517 (2009) 3143.
[10] F. Long, W.-M. Wang, H.-C. Tao, T.-K. Jia, X.-M. Li, Z.-G. Zou, Z.-Y. Fu, Mater. Lett. 64 (2010) 195.
[11] Q. Lu, J. Hu, K. Tang, Y. Qian, G. Zhou, X. Liu, Inorg. Chem. 39 (2000) 1606.
[12] D. Pan, L. An, Z. Sun, W. Hou, Y. Yang, Z. Yang, Y. Lu, J. Am. Chem. Soc. 130 (2008) 5620.
[13] J.S. Gardner, E. Shurdha, C. Wang, L.D. Lau, R.G. Rodriguez, J.J. Pak, J. Nanopart. Res. 10 (2008) 633.
[14] Y. Qi, K. Tang, S. Zeng, W. Zhou, Microporous Mesoporous Mater. 114 (2008) 395.
[15] X. Gou, F. Cheng, Y. Shi, S. Peng, J. Chen, P. Shen, J. Am. Chem. Soc. 128 (2006) 7222.
[16] K. Wakita, M. Iwai, Y. Miyoshi, H. Fujibuchi, A. Ashida, Compos. Sci. Technol. 65 (2005) 765.
[17] T. Pons, E. Pic, N. Lequeux, E. Cassette, L. Bezdetnaya, F. Guillemin, F. Marchal, B. Dubertret, ACS Nano 4 (5) (2010) 2531.
[18] M. Krunks, E. Kärber, A. Katerski, K. Otto, I. Oja Acid, T. Dedova, A. Mere, Sol. Energy Mater. Sol. Cells 94 (2010) 1191.
[19] M.G. Panthani, V. Akhavan, B. Goodfellow, J.P. Schmidtke, L. Dunn, A. Dodabalapur, P.F. Barbara, B.A. Korgel, J. Am. Chem. Soc. 130 (2008) 16770.
[20] Q. Guo, G.M. Ford, H.W. Hillhouse, R. Agrawal, Nano Lett. 9 (8) (2009) 3060.
[21] B. O'Regan, M. Grätzel, Nature 353 (1991) 737.
[22] Q. Pei, G. Yu, C. Zhang, Y. Yang, A.J. Heeger, Science 270 (1995) 719.

[23] E.W. McFarland, J. Tang, Nature 421 (2003) 616.
[24] U. Bach, D. Lupo, P. Comte, J.E. Moser, F. Weissörtel, J. Salbeck, H. Spreitzer, M. Grätzel, Nature 395 (1998) 583.
[25] P. Wang, S.M. Zakeeruddin, J.E. Moser, M.K. Nazeeruddin, T. Sekiguchi, M. Grätzel, Nat. Mater. 2 (2003) 402.
[26] M. Nanu, J. Schoonman, A. Goosens, Nano Lett. 5 (9) (2005) 1716.
[27] R. O'Hayre, M. Nanu, J. Schoonman, A. Goosens, Nanotechnology 18 (2007) 055702.
[28] J.M. Peza-Tapia, A. Morales-Acevedo, M. Ortega-López, Sol. Energy Mater. Sol. Cells 93 (2009) 544.
[29] R.H. Willens, Appl. Phys. Lett. 49 (11) (1986) 663.
[30] B. Mogwitz, C. Korte, L. Kienle, M. von Kreutzbruck, J. Janek, J. Appl. Phys. 101 (2007) 043510.
[31] C. Wang, Y. Li, X. Bu, N. Zheng, O. Zivkovic, C.S. Yang, P. Feng, J. Am. Chem. Soc. 123 (2001) 11506.
[32] J. Janek, B. Mogwitz, G. Beck, M. Von Kreutzbruck, L. Kienle, C. Korte, Prog. Solid State Chem. 32 (2004) 179.
[33] R. Bacewicz, W. Gebicki, J. Filipowicz, J. Phys. Condens. Matter. 6 (1994) L777.
[34] G. Morell, R.S. Katiyar, S.Z. Weisz, T. Walter, H.W. Schock, I. Balberg, Appl. Phys. Lett. 69 (1996) 987.
[35] E. Quiroga, W. Bensch, M. Aceves, Z. Yu, J.P. Savy, M. Haeckel, A. Lechner, 10th International Conference on Ultimate Integration of Silicon (ULIS 2009). IEEE, Aachen, Germany, 2009, p. 349.
[36] M. Winkler, O. Tober, J. Penndorf, K. Szulzewsky, D. Röser, G. Lippold, K. Otte, Thin Solid Films 361–362 (2000) 273.
[37] N.M. Gasanly, A.Z. Magomedov, N.N. Melnik, B.G. Salamov, Phys. Stat. Sol. B. 177 (1993) K31.
[38] H.L. Hwang, C.L. Cheng, L.M. Liu, Y.C. Liu, C.Y. Sun, Thin Solid Films 67 (1980) 83.
[39] C. Guillén, J. Herrero, M.T. Gutiérrez, F. Briones, Thin Solid Films 480–481 (2005) 19.
[40] E.G. Moshopoulou, R.M. Ibberson, J.L. Serrao, J.D. Thompson, Z. Fisk, Acta Crystallogr. B. 62 (2006) 173.
[41] L. Gastaldi, L. Scaramuzza, Acta Crystallogr. B36 (1980) 2751.
[42] M.E. Norako, M.A. Franzman, R.L. Brutchey, Chem. Mater. 21 (2009) 4299.
[43] K. Nose, Y. Soma, T. Omata, S. Otsuka-Yao-Matsuo, Chem. Mater. 21 (2009) 2607.
[44] M. Ben Rabeh, M. Kanzari, B. Rezing, Thin Solid Films 515 (2007) 5943.
[45] S. Peng, F. Cheng, J. Liang, Z. Tao, J. Chen, J. Alloys Comp. 481 (2009) 786.
[46] D. Abou-Ras, U. Jahn, M. Nichterwitz, T. Unold, J. Klaer, H.W. Schock, J. Appl. Phys. 107 (2010) 014311.
[47] Z. Wanga, X. Mo, J. Li, D. Sun, G. Chen, J. Alloys Comp. 487 (2009) L1.
[48] T. Sebastian, M. Gopinath, C. Sudha Kartha, K.P. Vijayakumar, M. Abe, Y. Kashiwaba, Sol. Energy 83 (2009) 1683.
[49] A.F. Qasrawi, N.M. Gasanly, Cryst. Res. Technol. 38 (12) (2003) 1063.
[50] A.F. Qasrawi, N.M. Gasanly, Cryst. Res. Technol. 36 (2001) 1399.
[51] R.H. Bube, Photoelectronic Properties of Semiconductors. Cambridge University Press, Cambridge, 1992.
[52] T.T. John, T. Sebastian, C. Sudha Kartha, K.P. Vijayakumar, M. Abe, Y. Kashiwaba, Physica B. 388 (2007) 1.
[53] D.K. Schroder, Semiconductor Material and Device Characterization. John Wiley & Sons, Inc., New York, 1998.
[54] J.M. Peza-Tapia, A. Morales-Acevedo, M. Ortega-López, 4th International Conference on Electrical and Electronics Engineering (ICEEE). IEEE, Mexico City, 2007, p. 326.
[55] G.C. Park, H.D. Chung, C.D. Kim, H.R. Park, W.J. Jeong, J.U. Kim, H.B. Gu, K.S. Lee, Sol. Energy Mater. Sol. Cells 49 (1997) 365.
[56] M.B. Read, J.H. Lang, A.H. Slocum, 55th IEEE Holm Conference on Electrical Contacts. IEEE, Vancouver, Canada, 2009, p. 303.
[57] Y. Akaki, H. Komaki, K. Yoshino, T. Ikari, J. Vac, Sci. Technol. A 20 (2002) 1486.
[58] Y.B. He, T. Krämer, I. Österreicher, A. Polity, B.K. Meyer, M. Hardt, Semicond. Sci. Technol. 20 (2005) 685.
[59] M. Mobarak, H.T. Shaban, A.F. Elhady, Mater. Chem. Phys. 109 (2008) 287.
[60] A. Amara, W. Rezaiki, A. Ferdi, A. Hendaoui, A. Drici, M. Guerioune, J.C. Bernède, M. Morsli, Sol. Energy Mater. Sol. Cells 91 (2007) 1916.